International Journal of Geo-Information

MDPI

Review

Parameters Derived from and/or Used with Digital Elevation Models (DEMs) for Landslide Susceptibility Mapping and Landslide Risk Assessment: A Review

Nayyer Saleem *, Md. Enamul Huq, Nana Yaw Danquah Twumasi, Akib Javed and Asif Sajjad

State Key Laboratory of Information Engineering in Surveying, Mapping and Remote Sensing, Wuhan University, Wuhan 430079, China; enamul_huq@whu.edu.cn (M.E.H.); nanatwumasi@whu.edu.cn (N.Y.D.T.); akibjaved@whu.edu.cn (A.J.); asifsajjad@whu.edu.cn (A.S.)

* Correspondence: saleemnayyer@whu.edu.cn; Tel.: +86-131-6411-7422

Received: 15.09.2019; Accepted: 27.11.2019; Published: 29 November 2019

Abstract: Digital elevation models (DEMs) are considered an imperative tool for many 3D visualization applications; however, for applications related to topography, they are exploited mostly as a basic source of information. In the study of landslide susceptibility mapping, parameters or landslide conditioning factors are deduced from the information related to DEMs, especially elevation. In this paper conditioning factors related with topography are analyzed and the impact of resolution and accuracy of DEMs on these factors is discussed. Previously conducted research on landslide susceptibility mapping using these factors or parameters through exploiting different methods or models in the last two decades is reviewed, and modern trends in this field are presented in a tabulated form. Two factors or parameters are proposed for inclusion in landslide inventory list as a conditioning factor and a risk assessment parameter for future studies.

Keywords: digital elevation models (DEMs); landslide hazards; landslide susceptibility mapping; landslide conditioning factors; landslide risk assessment

1. Introduction

Over the past three decades, developments in the field of computer vision, remote sensing and algorithms, have made it possible to conduct digital terrain analysis accurately in several types of analyses, assessments, and applications. Digital terrain analysis [1] is defined as, "collection, analysis, evaluation and interpretation of geographic information on the natural and man-made features of the terrain (elevation), combined with other relevant factors, to predict the effect of the terrain". Digital terrain analysis is usually performed to pursue the mathematical conceptualization of a terrain surface in order to describe landscapes and to define relationships between the terrain surface and several natural procedures and developments [2]. Terrain analysis plays an imperative role or provides the basis for risk assessment of natural hazards such as, flooding, landslides, earthquakes, ground liquefaction, tsunamis, typhoons, cloud bursting, and wild fires. In digital environments, terrain analysis is usually executed on mathematically expressed surfaces, generally known as digital elevation models (DEMs). In the following sub-sections, we will present a short review on DEMs, geo-information science and landslide hazards.

1.1. Digital Elevation Models (DEMs)

DEMs are considered one of the basic data sources for three dimensional modeling of the Earth's topography [3] and also suitable to provide a snap shot of landscape along with the available features having the elevation values [4]. DEMs have been defined as digital representations generated with elevation values at the equal grid intervals of the terrain [5–8]. The United States Geological Survey (USGS) [7] has also defined these models as a digital cartographic representation method for the elevation of the terrain at regularly spaced intervals x and y directions using z (elevation) values referenced to a common vertical datum. Land surveyed topographic maps, photogrammetry, Global Positioning System (GPS) observations, radar interferometry, Light Detection and Ranging (LiDAR), Radio Detection and Ranging (RADAR), and Interferometric Synthetic Aperture Radar (InSAR) are some of well-known resources for the extraction of digital elevation models [8–10]. A short preview of DEMs datasets is presented in Table 1.

Table 1. Digital elevation model (DEM) datasets information about involved methods and developers.

DEMs/Datasets	Methods/Products	Developers	Resolution	References/Access Information
Field Surveying Datasets	GNSS Observations	International collaborators, National mapping and research organizations, Geo-spatial analysts, etc.	Depends upon adopted method or applications requirements	[8–11]
	Field Levelling			
	Gravity Surveying			
Remote Sensing Datasets	Aerial and Satellite Imagery			
	Laser Scanning (LiDAR)		Less than 1 m	
	RADAR			
Topographic Maps	Contour Digitization		Depends on scale and contour interval of maps	[12–15]
Global Digital Elevation Models (GDEMs)	ASTER	NASA, USA and METI, Japan	30 m, 90 m	[16]
	SRTM	USGS, NGA and German and Italian Space Agencies	30 m, 90 m	[17]
	GTOPO30	USGS	30″	[18]
Gravitational Models	EGM 84/96/2008	NIMA, NASA and Ohio State University	30′ × 30′ (84) 15′ × 15′ (96) 2.5′ × 2.5′ (2008)	[19,20]
	WGM12	BGI, CGMW, IUGG, UNESCO, IAG, IUGS	02′ × 02′	[21]

GNSS: Global Navigation Satellite System, ASTER: Advanced Spaceborne Thermal Emission and Reflection Radiometer, SRTM: Shuttle Radar Topography Mission, GTOPO30: Global Digital Elevation Model with 30″ resolution, NASA: National Aeronautics and Space Administration, METI: Ministry of Economy, Trade and Industry, NGA: National Geospatial-Intelligence Agency, NIMA: National Imagery and Mapping Agency, BGI: Bureau Gravimetric International, CGMW: Commission for Geological Map of the World, IUGG: International Union of Geodesy and Geophysics, UNESCO: United Nations Educational, Scientific and Cultural Organization, IAG: International Association of Geodesy, IUGS: International Union of Geological Sciences, EGM: Earth Gravity Model, WGM: World Gravity Model.

Open source DEMs have replaced higher-resolution elevation models in a few applications, however, they are not feasible in applications that demand high accuracy. The accuracy of a DEM is always dependent on the quality of the field survey data collection methods [22], and these include contour insertion/plotting, scanning quality, digitization accuracy, map scale, and interpolation techniques. Parameters or characteristics claimed by researchers in the past to evaluate the accuracy of a DEM, include slope, aspect, curvature, RMSE, normal vector deflection, vertical and positional accuracy, and spatial resolution. Systematic errors appear during the data collection process, which ultimately affects the quality of a DEM; these errors have an effect on reliability of an application/assessment based on DEMs [9,23]. DEM-based applications/assessments are highly

concerned with the accuracy of model or the method by which these models are generated. However, the most accurate DEMs are also the costliest. To achieve sub-meter accuracy of elevation models, LiDAR, aerial photography and ground survey techniques are most suitable methods but at high unit cost [24]. To improve the accuracy of low-resolution DEMs (usually open source datasets), they are merged with DEMs at higher accuracy. However, the fusion of DEMs for the same region, acquired with different procedures, time windows, densities, scale, resolutions and accuracies is still not an easy assignment for achieving the desired results [25]. A short synopsis about the extraction of DEMs using different data sources are presented in Table 2.

Table 2. Examples of few DEMs data sources, exploited methods and achieved accuracies.

References	Region	Area (Km^2)	DEM Data Sources	Exploited Methods	Vertical Accuracy in Root Mean Square Error (RMSE)
Weng, (2002) [26]	Georgia, USA	13	Topographic contour maps Scale 1:24,000, contour interval 20 ft	SURFER Interpolation package	4.4–9.8 m
Chang et al., (2004) [27]	Australia	35	ALS DEM Photogrammetric DEM InSAR DEM	Comparison of DEMs with RTK GPS data	0.09–0.3 m 1.35–2.4 m 4.26–19.4 m
Webster et al., (2006) [28]	Nova Scotia, Canada	360	Aerial Laser scanning (LiDAR), Point spacing 3 m	Surface construction using TIN method	0.15–0.25 m
Zhang and Fraser, (2008) [29]	Hobart, Australia	120	IKONOS Geo Stereo Images	Image Matching using bi-cubic interpolation approach	2–6 m
Soycan and Soycan, (2009) [14]	Istanbul metropolitan city, Turkey	0.8	Topographic paper map sheets Scale 1:1000, contour interval 1 m	TPS Interpolation technique	0.02–0.40 m
Capaldo et al., (2012) [30]	Trento, Italy	50	GeoEye-1 and TerraSAR-X	RPF and RPC models for Optical & SAR Imagery	2.3–7.5 m
Mohd et al., (2014) [31]	Ampang & Hulu Langat, Malaysia	85	IfSAR, Topo map DEM	Digitization, Correlation of height points, Profiling, Visual comparison	1.5–3.0 m
Wu et al., (2015) [32]	Hong Kong	900	ZY-3, Pleiades-I, LiDAR data	Geometric Integration model for HRSI and LiDAR	3.3 m and 2.6 m
Yu et al., (2016) [33]	Guangyuan city, China	26,000	Google Earth Images	Terrain data extraction	55–80 m
Leitão and de Sousa, (2018) [34]	Switzerland	1	UAV imagery DEM, LiDAR DEM with 0.5 m spacing	Mergence of DEMs using MBlend method	0.4–0.6 m
Akturk and Altunel, (2018) [35]	Kastamonu, Turkey	0.02	UAV imagery, GPS point data	3D point cloud generation using Pix4D software	0.5 m

This table shows that accuracy increases with the decrease in spatial extent of study area and LiDAR based DEMs achieved better vertical accuracy amongst all. It also gives an overview of the spatial extent of extracted DEMs using different methods and vertical accuracy achieved in different parts of the world.

1.2. Geo-Spatial Information Science and Disasters

Space-based information is an effective and reliable source for disaster management, risk reduction, hazard observation, emergency response actions, evacuation, relief actions, and rehabilitation monitoring. However, for developing countries with limited resources, access to these types of datasets is limited. To cater the needs of disaster management authorities across the globe,

the United Nations General Assembly has passed a resolution (61/110 of 14 December 2006) with the establishment of the United Nations Platform for Space-based Information for Disaster Management and Emergency Response [36], as a program of the United Nations Office for Outer Space Affairs [37]. This platform facilitated to conduct a study report of the Value of Geo-information for Disaster Risk Management (VALID) [38], which provides assessment data along with scientific background information for geo-spatial products and services. This study traces the importance given by user community to geospatial information applications not only in emergency response but also for disaster-risk monitoring in terms of lowering public losses and refining risk reduction plans. In this report, they also discussed scientific and technical background of landslide hazard assessment and mapping based on DEMs using Geographic Information System (GIS). The mission statement of United Nations platform reads:

> *"Ensure that all countries and international and regional organizations have access to and develop the capacity to use all types of space-based information to support the full disaster-management cycle."*

With this mission statement and aid, developing countries can respond to catastrophic situations and disasters with efficient mitigation measures exploiting maximum available resources. Geo-spatial information enables city planners or management authorities to assess potential risks and devise appropriate policies to guide future urban growth [39,40]. High-resolution (both spatial and temporal) Earth observation satellites and innovations/developments in remote-sensing techniques/equipment, have enhanced the quality of landslide vulnerability assessments significantly [41,42], but timely DEM products at higher scale and accuracy are needed for these applications [43]. DEMs are not only applied in three-dimensional modeling of the Earth's topography but also in the analysis of geospatial phenomena [3,44]. DEMs are widely used as geospatial information sources for various remote-sensing applications, including precise ortho-rectification of high resolution satellite images, urban development studies, archeology, topography, tsunami assessments, glacier observations, geomorphology, plant cover research, 3D spatial analyses, multi-criteria decision support systems, hydrographic modeling, and deformation monitoring [45–47].

1.3. Landslide Hazards

The International Federation of Red Cross [48] has defined natural disasters as naturally occurring physical phenomena caused either by rapid or slow onset events, which can be geophysical (earthquakes, landslides, tsunamis and volcanic activity), hydrological (avalanches and floods), climatological (extreme-temperatures, drought and wildfires), meteorological (cyclones and storms/wave surges) or biological (disease epidemics and insect/animal plagues). In this paper, we consider only geophysical natural disasters (landslides) for discussion.

A landslide is defined as, "movement of a mass of rock or debris or earth down a slope" [49], and is considered as a catastrophic event across the globe, resulting in enormous damage to property and human life [50]. Considering their destructive nature, an effective mitigation plan for landslides should exist to minimize the loss of infrastructure, economic assets, and human life [42]. Landslides are often triggered by earthquakes or massive rainfalls in an area. However, these are not the only factors responsible for the initialization of landslides. Other factors can also play a role in the occurrence of such hazards. Interconnected factors such as lithology, topography, ground water conditions, ground stability, terrain morphological parameters (slope angle, orientation, altitude and curvature) and land cover are important for triggering landslides induced as result of earthquakes [51].

In the past, landslides occurred without warning and resulted in substantial damage to human settlements and life e.g., Las Colinas flow-like landslide triggered by the 2001 earthquake in El Salvador (Figure 1), caused a landslide of 800 m with a huge volume of 183, 500 m^3 claiming the lives of 485 people [52]. Similarly, almost 60,000 individual landslides were triggered by the Wenchuan earthquake in Sichuan Province, China on 12 May 2008 resulting in 20,000 deaths [53]. Due to the

devastating nature of landslide hazards, landslide hazard mapping or risk assessment of such hazards has become a motivating area of research. In order to lessen the damages caused by landslides, land developers must identify areas that are more susceptible to future landslide events in order to avoid such disasters in future; however, rapid climate changes and unplanned urban growth has increased the devastating risk for urban areas population and infrastructure day by day. The National Aeronautics and Space Administration (NASA) reported 11,033 landslide events triggered by rainfall across the globe (Figure 2) for the period 2007–2019 [54].

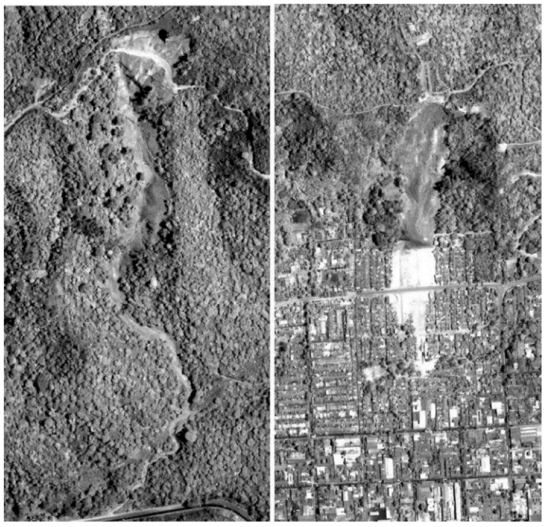

Figure 1. Landslide hazards events triggered by earthquake, occurred in El Salvador, 2001 [52].

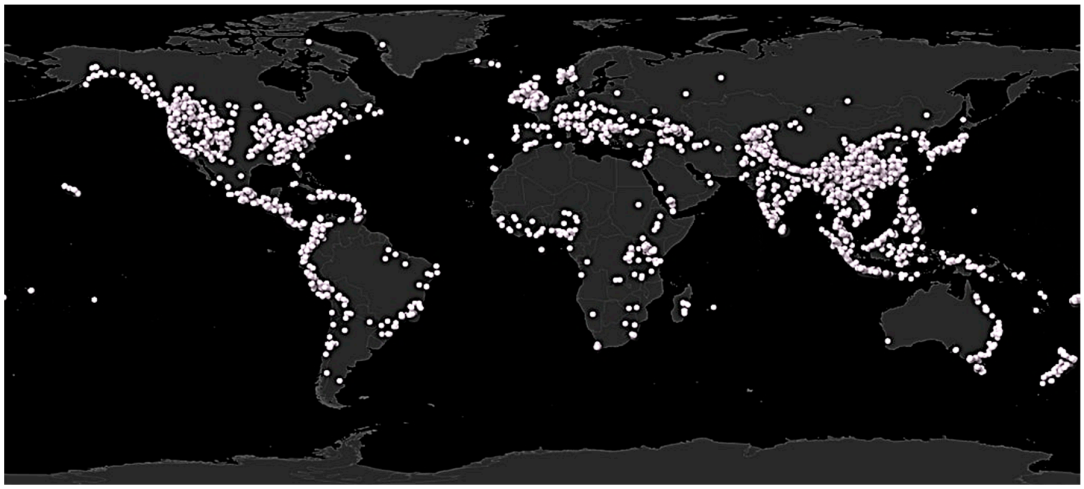

Figure 2. Rainfall triggered landslide hazard events catalog issued by the National Aeronautics and Space Administration (NASA) across the globe for the period 2007–2019 [54].

Computational models developed by researchers for prediction and monitoring of natural phenomena e.g., erosions, landslide occurrence, hydrological modeling, etc. are generally dependent on the digital elevation models acquired from different sources [55]. DEMs along with their attributes and properties including topographic index, curvature, drainage network, slope, aspect, etc. make available the parameters for information extraction and assessment of any process involving terrain analysis [56]. Combination of various photogrammetric procedures, remote-sensing algorithms and GIS tools make possible to some extent the identification of areas vulnerable to future landslide events through the development of landslide inventories along with parameters. DEMs, either developed form a single source or obtained through fusion of multi-source data, are most suitable for creating the models required for such risk assessments. In the following

sections of this paper, the relationship between parameters derived from DEMs and their impact on risk assessment for landslide hazard will be discussed.

2. DEMs Parameters Exploited for Landslide Hazards Risk Assessment

Risk assessment for geophysical hazards like landslides, depends on probability estimation of frequency, magnitude of future events, and their adverse consequences [57]. Urban settlements in flat areas are generally not affected by landslide hazards but settlements in hilly areas or near to hilly areas are often affected by these hazards. Risk is defined as a function of both hazard and vulnerability [50], and it can be calculated as:

$$R = P_f . v . n_p \quad (1)$$

where P_f represents the regional probability of a slope failure, ranked from 0 (not possible) and 1 (certain); v represents the physical and socioeconomic fragilities of the affected communities in terms of degree of loss, ranked from 0 (no loss) to 1 (complete loss); and n_p represents the number of people exposed to potential landslides.

Landslide risk is expressed as a probability that an area will undergo substantial levels of damage from a landslide event [50]. To assess the risk of landslide hazard in an area, the topography is visualized in a digital environment as DEMs and their extraction through several existed procedures is important. Being an important source of information for many other applications, DEMs have also found applications in identifications of topographic settings susceptible to land sliding [58]. Further derivations from DEMs are usually employed for the assessment of landslide hazard risk. Employment of these derivations are further utilized in statistical analysis at regional scales (slope gradient, slope direction, slope length and curvature), in landslide run out modeling (flow path and rock fall movement), in empirical analysis at small scales (internal relief, drainage density and hill-shading images). Basic mapping units of these derived maps are exploited for analysis within many statistical approaches. These mapping units are either grid cells, slope aspects or exceptional units which are made by other landslide inventory elements e.g., land cover, slope gradient, curvature and lithology [59]. In the modern digital environment, DEMs are considered as an important source of data for provision of critical indicators, which have imperative and basic role during the risk assessment of landslide hazards [60]. A short introduction of few of these indicators, is presented here in the following sub-sections.

2.1. Slope (Angles, Gradient and Aspect)

Digital elevation models are exploited efficiently for prediction of regional distribution of slope angles in order to assess slope instability levels for the region [61]. Elevation being the variable in elevation models, therefore slope is considered as first derivative of the elevation, which is calculated to quantify variation in elevation over a distance. Slope is an imperative indicator of a DEM for certain applications e.g., water flow management, landslide feasibility, etc. Geometrically, slope is a property attached with the line and is defined as, "flexible tangent of the angle made by a straight line with the x-axis"[62]. Slope of a line can be positive, negative, nil, etc. (Figure 3). [63] defined slope based on their categorized representations and are described hereunder:

$$\begin{aligned} Slope &= Rise/Run \ \ (Geometric\ Ratio) \\ &= (y_2 - y_1)/(x_2 - x_1) \ \ (Algebraic\ Ratio) \\ &= mx + b \ (Parametric\ Ratio) \end{aligned} \quad (2)$$

This parameter was used in Ref. [64, 65] to measure image intensity and reflectance for a given surface orientation. In terms of surface modeled by a DEM, slope is defined as tangent plane to that surface at a point [66]. Slope was classified in Ref. [67] into two components i.e., gradient and aspect, whereas, gradient is defined as maximum rate of change in altitude and aspect is the compass direction of this maximum rate of change. The author applied and compared six algorithms for calculating gradient and aspect for a DEM generated for a medium topography with regular 30 m

grid spacing. One of the algorithms made use of second-order finite difference method for a 2 × 2 moving window. After initial steps, the gradient is calculated with the help of following formula:

$$\tan G = \sqrt{(\delta z/\delta x)^2 + (\delta z/\delta y)^2} \quad (3)$$

where G represents slope gradient at point (i, j). Aspect, which is the direction of maximum slope is calculated as;

$$\tan A = (\delta z/\delta x)/(\delta z/\delta y) \quad (4)$$

where,

$$\left[\frac{\delta Z}{\delta x}\right]_{(i,j)} = \frac{\left[\left(Z_{i+1,j+1} + 2Z_{i+1,j} + Z_{i+1,j-1}\right) - \left(Z_{i-1,j+1} + 2Z_{i-1,j} + Z_{i-1,j-1}\right)\right]}{8\Delta x},$$

$$\left[\frac{\delta Z}{\delta y}\right]_{(i,j)} = \frac{\left[\left(Z_{i+1,j+1} + 2Z_{i,j+1} + Z_{i-1,j+1}\right) - \left(Z_{i+1,j-1} + 2Z_{i,j-1} + Z_{i-1,j-1}\right)\right]}{8\Delta y}$$

The topographic parameters obtained from DEMs are slope and aspect (direction of slope), and these parameters can be further used to calculate upslope area and topographic index [68]. It was proclaimed by Ref. [50] that slope stability level is highly influenced by not only intrinsic factors (soil composition, moisture level, etc.) but also extrinsic factors (rainfall intensity, seismic activity, etc.). Another factor related with slope angles is their distribution in the area. According to [69], slope angles are important indicator for slope stability and regional landslide hazards are critically dependent upon slope angles distribution throughout the region. In a digital environment, DEMs are stored as regular or irregular gridded cells, and the adjacency of these cells forms a surface for provided elevation values. Slope angle for each cell is estimated using elevation values in relation to its neighboring cells. Values of slope angles derived from DEM are dependent upon the resolution of DEM [61]. Slope angles, gradient and aspect values obtained from a DEM have placed these data in a focal position in landslide hazard risk assessment.

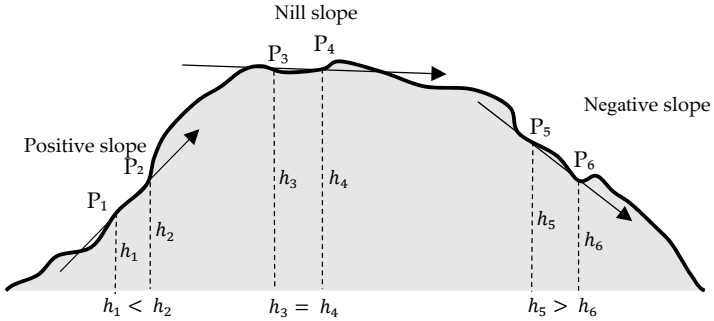

Figure 3. Different values of slope according to terrain.

2.2. Curvature

The curvature parameter is computed from the existing slopes between two elevational surface points. It was initially proposed by [70], for quantitative analysis of land surface topography. Curvature is a second derivative of elevation and measure of change of slope between two points over a distance (Figure 4). Curvature is used to measure deviation from a straight line [62]. Let A be the arc length between two points P1 and P2 and angle between both slopes (tangents) is α, then the curvature between two points can be calculated as;

$$\kappa = \lim_{A \to 0}(\alpha/A) = d\alpha/dA \quad (5)$$

If A becomes so small, physically meaning that both points are almost at the same location (in this case height), the resultant deviation becomes also negligible and curvature for those points becomes zero. The curvature between two points located on a flat surface always has a zero value, since the slope between these points is parallel. Like slope, curvature also has positive (concave) and negative (convex) values, depending upon the terrain. Curvature has been used extensively by

several researchers e.g., [67–72], etc. in previous studies conducted for the prediction of zones prone to future land slide hazards events. For example, [72] used curvature along with other parameters for the evaluation of frequency ratio and logistic regression model in order to create GIS-based landslide-susceptible maps. Three types of curvature functions are defined in the GIS environment [73]. They highlight different aspects of the slope and include profile, plan, and standard curvature. Profile curvature and plan curvature are parallel and perpendicular to the direction of maximum slope, respectively indicating the direction of maximum slope. Profile curvature measures the flow acceleration/deceleration, while plan curvature is related with convergence/divergence of flow across the surface. Standard curvature combines both the profile and plan curvatures, which provides better understanding of flow across the surface.

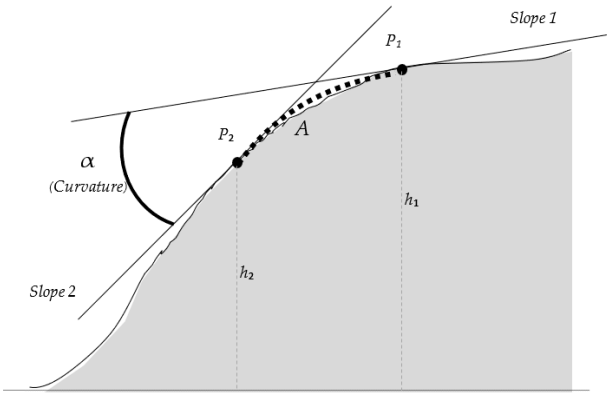

Figure 4. Curvature (α) between two points.

2.3. Topographic Position Index (TPI)

The topographic position index (TPI) is computed as difference between the cell elevation and the mean elevation of neighboring cells [74]. However, to categorize existing topographic landforms i.e., valley, slope, and ridge, specific values of thresholds are needed to be defined. The concept of TPI was presented by [75] for landforms analysis with the notion that landform classifications are derived from the ranges of TPI values. TPI along with lithology is an effective factor for debris flow and also describes the expression of the geomorphological settings (slope, ridge, valley, etc.) in a quantitative way [60]. It is also considered as a geomorphological landslide conditioning parameter, as landslide events usually take place on the ridges [76]. Like other indices, TPI has also been exploited extensively in many functions, models, and methods developed by researchers e.g., [72–77], etc. for landslide susceptibility. A detailed method was developed by [78] for the calculation of TPI in their study of land facet corridor design and has been added in ArcGIS software as an extension [79]. Recently, [80] published their research about the effective identification of terrain positions from gridded DEM, which includes local and regional terrain attributes based classification methods. TPI was used in their study to identify terrain positions, ridge, shoulder, lower flat, valley, hillock, and side slope, etc.; these values were found to be consistent with the actual local and regional topography of the area.

2.4. Topographic Wetness Index (TWI)

The topographic wetness index (TWI) is dependent on slope largely and is generally exploited in studies of hydrological processes. It is a commonly used tool to forecast the amount of soil moisture at the catchment scale and allows the analysis of topographic control on hydrologic response of a watershed [78–80]. Topography is a factor for landslide hazards, and therefore indices related with topography have always been employed for data analysis performed for various applications [55].

TWI was initially proposed by [83], along with the topography based hydrological model (TOP-MODEL) and can be calculated as:

$$\mathrm{TWI} = \ln(a/\tan\beta) \quad (6)$$

where a is the local upslope area draining through a certain point per unit contour length and $\tan\beta$ defines the local slope. Many researchers evaluated TWI in terrain analysis. Ref. [81] derived TWIs using dynamic hydrological model to predict spatial patterns of saturated areas and claimed the improvement in prediction of spatial distribution of wetlands substantially better than the TWIs derived by other means in catchments. Ref. [82] developed a modified TWI computation procedure for depression-dominated areas exploiting DEM. Statistical analyses of TWI reveals that an interpolated DEM led to wrong quantity and distribution of TWI for depression dominated landscapes. Ref. [84] claimed that the topographic wetness index is reliable not only to examine the pattern of potential soil moisture in the field but also reliable for the detection of changes in soil texture caused by an erosion process. Ref. [85] suggested modifications in the existing algorithms for TWIs, concluding that TWI ability was sensitive with the algorithms used for upslope calculation contributing area and slope gradient in order to foresee observed patterns. Similarly, [86] equated computation methods of TWI, and evaluated them with measuring variables using correlation techniques. Ref. [87] computed TWI using multi-resolution DEMs and proposed an approach by adapting a multiple flow routing algorithm to utilize maximum downslope gradient as β. Ref. [88] also calculated TWIs using multi resolution DEMs with different vertical accuracies at central NY, USA, for agricultural landscapes.

2.5. Topographic Roughness Index (TRI)

As appeared from the nomenclature, the topographic roughness index (TRI) is in contrast to the TWI and is responsible for quantifying ruggedness of the terrain. TRI is considered as a morphometric measure which describes heterogeneous condition of a land surface [89]. TRI extracted from DEM facilitate in characterizing the terrain as smooth or rugged landforms and it portrays the local variance of surface gradients or curvatures [90]. Computation of TRI was initially proposed by [91], to quantify topographic heterogeneity through estimation of variability of elevation or slope in a local neighborhood. Their model simply computed TRI values for each grid cell of DEM using a Data Only Cells "DOCELL" command in ArcGIS, which calculates the sum change in elevation between a grid cell and its eight neighboring grid cells. Later on, other researchers have modified their approach by using other statistical measures for different analyses. Ref. [92] modified it through computation of root mean square of elevation, relief and slope. Similarly, [93] proposed a method to compute roughness by estimating the standard deviation of local slope of every cell according to its neighbors. In order to compute roughness, [94] introduced a method by calculating standard deviation of difference between topographic elevation and locally smoothed derivatives.

2.6. Sediment Transport Index (STI)

Another factor attached with DEM is called the sediment transport index (STI) or sometimes termed as the sediment transport capacity index. This index is directly related to the delivery of sediments from terrain into the channel during landslide events. The amount of sediment in a catchment indicates the potential sediment supply to the debris at the catchment mouth [57]. This potential varies according to the terrain, maximum slope angle distribution, rock formation, catchment area size, quantity and span of event, length of the debris movement. Ref. [95] proposed an approach to compute sediment transport capacity index through proposing an equation based on dimensional analysis. In their approach, rainfall data is also taken into account as a realistic feature, therefore a new equation is termed as a function of rainfall impacted stream power and slope. The estimation of sediment transport capacity index is necessary to develop soil erosion models [95]. It was first introduced by [96] in their work on unit stream power. It is dependent on catchment area and slope angle and can be computed as:

$$STI = (m+1) * (a/22.13)^m * (\sin\beta/0.0896)^n \quad (7)$$

where a is the local upslope area (catchment area), β is the slope angle, m is 0.6 and n is 1.3 [97]. It remained part of the assessment for susceptibility mapping for the last two decades and a short summary is presented here for an overview. Qualitative examination of the applicability of sediment transport capacity models was performed by [98], using main variables i.e., unit stream power, stream power and shear stress. This analysis reveals that the unit stream power model gives better simulation outcome on mild slopes, whereas stream power and shear stress models works fine with steep slopes. Along with other conditioning factors, [99], used STI in their study of susceptibility mapping of landslide hazards using bivariate (certainty factor and index of entropy) and multivariate (logistic regression) models. Factors used in their study were computed through topographic map, drainage map, road map and geological map. Similarly, [100] evaluated the results obtained through a statistical index and index of entropy methods for landslide susceptibility mapping. They have exploited STI along with twelve other landslide responsible factors in their analyses and their results have shown that success rate of index of entropy method is slightly better than statistical index using the area under the curve (AUC) method.

2.7. Stream Power Index (SPI)

The stream power index (SPI) is a conditioning factor related with DEM and used extensively for landslide susceptibility models along with other factors. It is a measure of the erosive power of flowing water. It was initially put forward by [101]. Later, [55] further examined this factor and also proclaimed that both SPI and TWI, when used jointly are trustworthy indicators of temporary gullies in agricultural watersheds. SPI can be computed as;

$$SPI = a * \tan\beta \quad (8)$$

where a is the local upslope area (catchment area) and β is the slope angle. The SPI parameter is widely used [67,69,78,102–107].

After the extraction of parameters/factors responsible for landslide event, already developed models/algorithms have been used for final output (susceptibility mapping). However, due to dissimilar dimensions of factors, simple summation is not possible and this is being done through statistical measures. Initially, different models (probability analysis, frequency ratio (FR), etc.), are exploited to establish a relationship between the landslide location and each landslide conditioning parameter. Correlation scores have been computed from the analysis of relationship between the landslides and related factors. On the basis of correlation scores, each factor's type or range has been finalized and rating of that factor has been made. For example, in the FR method, the rating of each factor is computed through an analysis of the relationship between the landslide and that factor's type. This value is ratio of number of cells where events did not take place to number of cells where landslide events did take place. The landslide susceptibility index (LSI) can be quantified by summation of each factor's rating/score through equation [104,105]:

$$LSI = \sum LCF_i \quad (9)$$

where, LSI is landslide susceptibility index and LCF_i is rating/score of each landslide conditioning factor/parameter. Parameters or indicators derived from or used with DEMs are discussed, which have been developed, refined, exploited and evaluated over the last two decades for landslide hazards susceptibility mapping. Interdisciplinary advancement and development of new approaches/models bring more factors in this domain. Other parameters used by the researchers include geological, and environmental parameters, e.g., distance to roads, distance to rivers, drainage density, distance to faults, land use, land cover, soil, cumulative rainfall, normalized difference vegetation index (NDVI), and lithology of an area.

3. Impact of Scale, Resolution and Accuracy of DEM on Parameters

Landslide susceptibility and landslide risk assessment studies depend on the resolution, scale and accuracy of a DEM, since these models serve as basic source to extract the parameters used for these studies. Landslide conditioning parameters are interconnected and dependent on each other i.e., curvature is dependent on the slope. Derivation of these parameters and their interpretation depends on the DEM resolution and scale. The DEM resolution refers to horizontal and vertical spatial information recorded in the database [108]. A large-scale DEM at fine resolution, can depict detailed topographic features of the terrain, therefore indicators extracted from finer DEMs are more reliable. Similarly, regions identified by high-resolution DEMs are considered more trustworthy due to the reliability of the parameters. The spatial resolution of an elevation model has a direct effect on the accuracy and quality of landslide susceptibility maps [109]. Ref. [110] documented resolution dependencies in terrain analysis using DEMs and their variation across landscape locations. Terrain attributes slope, plane curvature, profile curvature, north-south slope orientation, east-west slope orientation and topographic index, were evaluated as a function of DEM resolution. In terms of location and elevation values, sampled points matched exactly in the compared resolutions, however a regression analysis showed sensitive responses for each multi-resolution attribute. Further expanding their work, relationship of topographic parameters and spatial resolution was determined [2] finding that change in spatial resolution, affects not only point-specific terrain attributes but it also changed the meanings of topographic attributes at each point (Figure 5). Therefore, the impact of DEM resolution on terrain attributes could not be predicted through spatially aggregated statistical analysis, thus a spatially explicit approach is required. Furthermore, resolution resampling yielded a substantial difference in number and location of points, which weakened the accuracy of aggregated comparisons between different resolutions.

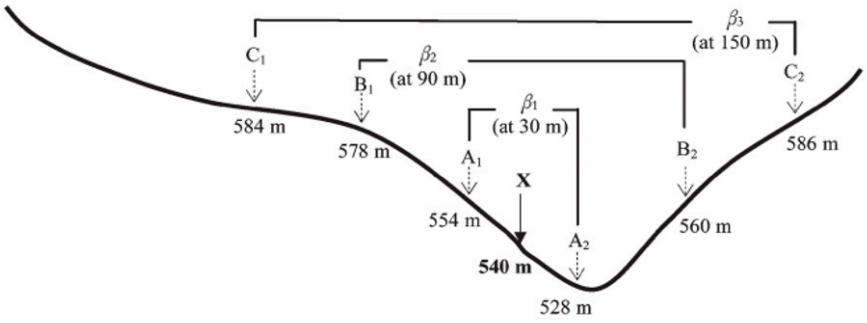

$$\beta_1 = \frac{(554m - 528m) \times 100\%}{30m} = 87\%, \quad \beta_1 \text{is the slope gradient for X at 30m spatial resolution, pointing from } A_1 \rightarrow A_2$$

$$\beta_2 = \frac{(578m - 560m) \times 100\%}{90m} = 20\%, \quad \beta_2 \text{is the slope gradient for X at 90m spatial resolution, pointing from } B_1 \rightarrow B_2$$

$$\beta_3 = \frac{(586m - 584m) \times 100\%}{150m} = 01\%, \quad \beta_3 \text{is the slope gradient for X at 150m spatial resolution, pointing from } C_2 \rightarrow C_1$$

Figure 5. Scale effects of terrain analysis. Slope gradients (β_1, β_2 *and* β_3) for the same point X are defined in different ways due to the change of spatial resolution. The resultant slope gradients are different not only in magnitude but also in topographic meaning (Deng et al., 2008).

Ref. [61] argued that slope angle for each cell is estimated using elevation values in relation to its neighboring cells, therefore slope angle values derived from DEMs depend upon the DEM resolution. Ref. [69] analyzed the critical scale related with landslide hazard, whereas critical scale is defined as a scale at which slope failures occur; the minimum size that a landslide event takes place and results in visible damage. Slope-gradient maps for landslide hazard assessment are dependent on the resolution of DEMs; a landslide is not disastrous if slope failure occurs in 1 m × 1 m cell size but not in surrounding cells and considered catastrophic if it happens for a cell of 1000 m × 1000 m. Ref. [82] assessed DEM resolution impact on developed TWI method for the depression dominated areas and concluded that filled DEM led to misleading quantity and distribution of TWI for such

landscapes. Ref. [88] used mixed effects modeling approach, with the claim that finer DEM are suitable for parameter extraction than coarser DEM. Resolution and scale not only affect the topographic parameters in these studies but DEM source also influences the desired parameters.

Vertically accurate DEMs yields realistic results but an error in grid elevation can lead to wrong model predictions or can affect the values of conditioning factors derived from a DEM. Quality of hydrological features was compared by [111], using 25 m contour-based DEM and 25 m re-sampled LiDAR-derived DEM. This comparison showed that LiDAR-based DEM depicted better presentation of hydrological features even after resampling of model. Ref. [112] examined the mean slope variation of a DEM using its resolution and LiDAR point density (2 m–10 m). Sensitivity analysis between modeled terrain slope and LiDAR point density exposed that the deviation between the mean slope and modeled mean slope decreases with thick point density and finer resolution. They concluded that the mean slope of elevation behaves as a linear function in relation to the cell size and as a logarithmic function with point-spacing. However, cell size influences the mean slope more than the point density. Other modern technologies are also being used by the researchers along with LiDAR based DEMs for landslide monitoring studies. For example, [113], used persistent scatterer interferometric synthetic aperture radar (PSInSAR) to analyze the effectiveness of LiDAR data for landslide study. Resolution and vertical accuracies exploited by the researchers with different data sources of DEMs for landslide monitoring evaluation studies are presented in Table 3.

Table 3. Resolution and vertical accuracies of DEMs for landslide monitoring evaluation studies.

References	Data Sources		Data Format	Resolution	Vertical Accuracy
Pesci et al., (2004) [114]	Aerial Photogrammetry	1:5000	Regular grid	6–12 cm	20–30 cm
		1:35,000	Regular grid	0.5–1.0 m	>1.0 m
	Terrestrial Photogrammetry	1:500	Regular grid	7–15 mm	~3 cm
		1:2000	Regular grid	2.5–5.0 cm	>5 cm
	Terrestrial Laser Scanning		Irregular grid	~0.5 cm	<5 cm
	Aerial Laser Scanning		Irregular grid	~10 cm	>10 cm
	GPS Kinematic		Irregular grid	~20 cm	~10 cm
Vaze et al., (2010) [111]	LiDAR		Irregular grid	1.0 m	~30 cm
Mclean, (2011) [69]	SRTM		Regular grid	90 m	~10 m
Dlugosz, (2012) [108]	Aerial Photogrammetry	1:13,000	Irregular grid	1.0 m	1.5 m
Ciampalini et al., (2016) [113]	Contour line interpolation		Irregular grid	20.0 m	-
	LiDAR	4–8 pt/m²	Irregular grid	1.0 m and 2.0 m	-
Mahalingam et al., (2016) [115]	Re-sampled LiDAR	7 pt/m²	Irregular grid	10.0 m	~4 cm
Chang et al., (2016) [116]	ASTER GDEM		Regular grid	30.0 m	-
Pawluszek and Borkowski, (2016) [103]	LiDAR	4–6 pt/m²	Regular grid	5.0 m	~0.20 m

DEM accuracy, resolution and scale influence landslide monitoring evaluation studies. Resolution and vertical accuracies of previously used DEMs involved in landslide mapping studies are presented in Table 3. LiDAR based DEMs are the best elevation models for these studies and a trend of involvement of other datasets with LiDAR datasets is also underway [113]. Crucial information is extracted from high resolution elevation models but often results in inaccurate interpretations of landslide susceptibility maps across a larger scale [115]. Furthermore, higher spatial resolution does not always guarantee a higher rate of prediction accuracy [109]. Therefore, an optimum DEM resolution for susceptibility studies depends upon the available data sources, methods, and terrain. Data acquisition methods are not free from measurement or systematic errors,

therefore subsequent products like DEM interpolation models are also affected by inherited errors or may be a source for the propagation of errors [9,23]. DEMs quality is dependent on field survey data collection techniques and the contour insertion/plotting, scanning quality, digitization accuracy, map scale, and interpolation techniques [117]. This dependency affects the quality of DEM based parameters used in susceptibility studies. Therefore, DEM sources selection and methods for extraction or attachment of parameters should be consistent with the terrain, spatial extent, and requirements of the application.

4. Landslide Hazards Susceptible Mapping Based on DEM Parameters

Disaster management authorities want to optimize the probability of accurate zonation mapping for landslide hazard events. Topography of an area prone to these hazards plays a significant role. In a GIS environment, zonal mapping of landslide hazards depends on accuracy, resolution, and the scale of the DEMs used for parameter extraction. Several algorithms have been developed using DEMs and parameters obtained from or attached to the susceptibility mapping of landslide hazards and risk assessment. Trends in this field for the last two decades are discussed in the upcoming paragraphs.

Ref. [118] described use and effectiveness of GIS in prediction and monitoring of landslide hazards. [119] made use of fuzzy relations for the production of landslide susceptibility maps using a landslide inventory database which is compiled by field surveys and aerial photographs analysis. Ref. [120] used rough set theory to extract rules describing the bond between landslide-conditioning factors and landslide events. In their study, landslide susceptibility is derived from decision rules in rough set analyses and presented maps of areas with roads and without roads. Advancements in the machine learning field attracted researchers, therefore, [121] compared logistic regression and neural networks methods for a medium scale study to produce susceptible maps. Due to a higher compatibility rate between field observations and the results obtained through analyses, neural networks results seems more realistic for the study area. Similarly [122] used artificial neural networks (ANN) for landslide susceptibility through computation of parameters on ASTER DEM. Ref. [72] evaluated the performance of FR and logistic regression (LR) models with the claim that the LR model performed better than the FR model in comparison to its accuracy for ratio of landslide validation. Ref. [123] integrated frequency ratio (FR) and certainty factor (CF) techniques to validate spatial prediction models by structural similarity and processing eight factors. In their approach, FR performs better than CF in terms of validation. Ref. [124] used a certainty factor (CF) model and logistic regression (LR) model for large-scale assessment of landslide hazards risks and vulnerability. In the last three discussed research works, three models i.e., FR, LR and CF were integrated with different combinations for landslide susceptibility.

To present an overview of the topographical parameters using statistical measures, the research work of [125], is discussed here as a case study. Ref. [125] configured the alterations to seed cell sampling strategy for landslide susceptibility assessments in order to generate landslide susceptible maps. A DEM was generated through digitization of contours (25 m interval) existing on topographical maps of scale 1:25,000. Sensitivity analyses were conducted on the topographical parameters derived from the DEM. Thematic and tabular forms of these parameters/indicators are depicted in Figure 6 and Table 4, respectively. Neighboring regions of maximum altitude values share high values for the slope, LS and SPI values, whereas TWI shows an inverse behavior. Plane and profile curvature involves positive and negative values, indicating the concavity and convexity of the terrain. Mean elevation and slope values of a landslide area and seed cells of 100 m are almost identical, which shows that landslides in the study area occurred in grid cells with lower altitudes with lower slope angles. The discussed values are made bold and underlined in Table 4.

Complexities of models or algorithms and number of parameters are enhanced to obtain more reliable results about landslide hazards susceptibility mapping. Ref. [126] evaluated the performance of three approaches i.e., statistical index (SI), index of entropy (IoE) and weight of evidence (WoE) using systematic comparison and validation by exploiting 13 parameters. Ref. [127] used a weight of evidence (WoE) method exploiting 12 parameters and claimed that performance of WoE approach remains the most accurate when training datasets and validating datasets for a study

area. A comprehensive review of statistically-based landslide susceptibility models was conducted by [128]. Recently, Ref. [129] exploited 18 parameters i.e., elevation, slope aspect, slope angle, profile curvature, plan curvature, STI, SPI, TWI, land use, NDVI, rainfall, lithology, distance to faults, fault density, distance to roads, road density, distance to rivers, and river density. They employed population-based evolutionary algorithms and a neuro-fuzzy approach to model landslide susceptibility. Parameters employed within the last three decades for susceptibility using different DEMs data sources and exploited methods or algorithms are summarized in Table 5. Qualitative measures are also presented for different models presented here which indicates the quality of results obtained for landslide hazards studies.

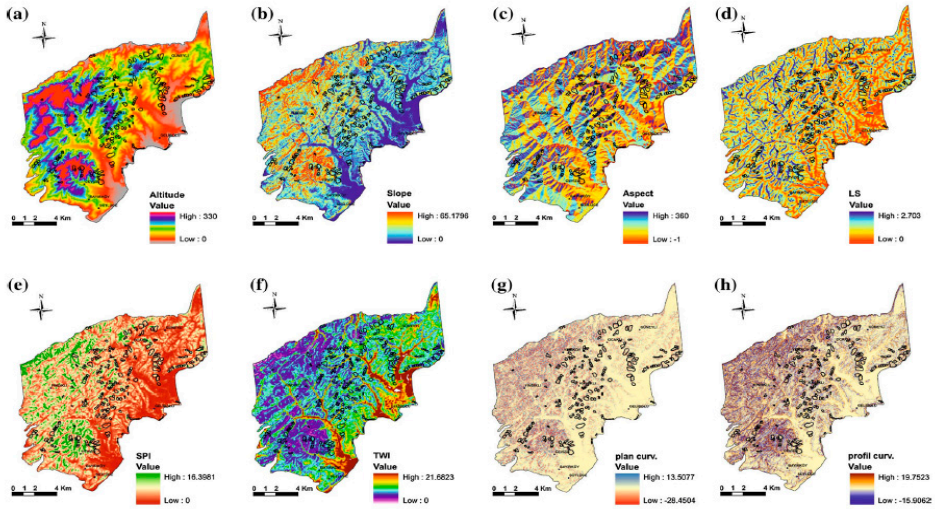

Figure 6. Topographical parameters used in landslide susceptibility assessment. (**a**) Altitude, (**b**) Slope, (**c**) Aspect, (**d**) Sediment transport capacity index (LS), (**e**) Stream power index (SPI), (**f**) Topographic wetness index (TWI), (**g**) Plan curvature, (**h**) Profile curvature [125].

Table 4. Descriptive statistics of topographical parameters used by Dagdelenler et al., (2015).

	Parameters	Min.	Max.	Mean	Std. Deviation	Variance	Skewness
Whole Study Area	Elevation	0	330.00	97.68	68.22	4653.99	0.68
	Slope	0	65.18	9.12	6.91	47.76	1.035
	Plan Curvature	−28.45	13.51	0.01	0.41	0.17	−1.82
	Profile Curvature	−15.91	19.75	0.01	0.46	0.21	0.42
	TWI	0	21.68	5.76	1.16	1.34	1.45
	SPI	0	2.70	0.55	0.39	0.15	0.98
	STI	0	16.40	1.44	1.23	1.51	1.91
Only Landslide Area	Elevation	0	301.30	92.35	53.12	2821.56	0.84
	Slope	0	38.65	9.95	4.69	21.96	0.80
	Plan Curvature	−3.20	2.51	−0.02	0.31	0.10	−0.49
	Profile Curvature	−2.27	3.49	0.03	0.35	0.12	0.90
	TWI	4.14	7.91	5.43	0.53	0.28	0.98
	SPI	0.03	2.16	0.65	0.31	0.28	0.77
	STI	0.92	8.40	1.67	0.87	0.76	1.50
Seed cell (buffer distance d = 100 m)	Elevation	0	312.82	114.59	57.62	3320.26	0.63
	Slope	0	41.47	10.08	5.48	30.04	0.82
	Plan Curvature	−3.65	3.48	0.032	0.36	0.13	−0.60
	Profile Curvature	−3.51	3.17	−0.06	0.40	0.16	−0.01
	TWI	4.01	9.47	5.33	0.51	0.26	0.77
	SPI	0	2.11	0.47	0.33	0.11	1.09
	STI	0	7.92	1.44	0.95	0.90	1.49

TWI: Topographic Wetness Index, *SPI:* Stream Power Index, *STI:* Sediment Transport Index.

Landslide conditioning parameters will keep their prominence in susceptibility studies and their quality and complexity affects the reliability of results achieved. With the help of the review

presented by [128] and literature shown in Table 5, an increasing trend can be observed towards involvement of machine learning methods in development of landslide-susceptibility models. However, complex models with more conditioning factors or parameters are interesting research area for the researchers to optimize the reliability of susceptibility mapping. Landslide susceptibility based on DEMs is extremely helpful for the authorities responsible for future development especially in terms of human settlement expansion management. Therefore, it seems beneficial to involve geo-spatial researchers or consider geo-spatial information research for disaster risk assessment and management.

Table 5. Selected references showing exploited parameters, DEMs data sources, methods and obtained results for landslide susceptibility mapping in the past.

References	Parameters	DEMs	Method	Results
	Exploited	Data Source	Used	
Carrara et al., (1991) [130]	Altitude, Slope aspect, Geological units	Topographic maps of scale 1:25,000 with 20 m contour interval	Discriminant analyses	Landside hazard risk is evaluated in each slope unit and is declared a cost-effective approach. **Classification Results**: 83.4% correctly classified 16.6% misclassified.
Gao (1993) [58]	Slope orientation, Slope gradient, Slope form/curvature	Topographic maps of scale 1:24,000 with 24 m contour interval	Analyses of landslide and topographic data, chi-squares test	Topographic variable are statistically significant to spatial distribution of the sites disturbed by landslide paths.
Pesci et al., (2004) [114]	Landslide morphology, Vegetation, Atmospheric environment and shadows	Photogrammetry, GPS and Laser scanning	Residual comparison analyses	Discussed three techniques are efficient to define landslide topography and morphological changes.
Nichol and Wong, (2005) [131]	Slope, Land cover, Geology	Satellite Imagery, Topographic maps with 10 m contour interval	Change detection and Image fusion	Detailed interpretation of landslides and attached features by combining two levels of survey for regional scale landslide monitoring. 70% of landslides were detected in the area with 20 m SPOT images.
Yilmaz, (2009) [104]	Elevation, Slope angle, Slope aspect, TWI, SPI, Geology, Faults, Drainage System	Topographic Maps of Scale 1:25,000	Frequency ratio, Logistic regression, ANN	Susceptibility map obtained from ANN model is more accurate than other models. **Validation Results**: FR ~82.6%, LR ~84.2%, ANN ~85.2%
Miner et al., (2010) [132]	Slope aspect and degree of slope, Plan and profile curvature, Flow accumulation, Terrain hill-shading, TWI, TRI	LiDAR based DEM	Landslide recognition process using DEM	LiDAR-derived DEM has proven itself a cost effective approach against traditional Aerial Photo Interpolation (API) and 10 times large area can be assessed.
Pourghasemi et al., (2012) [133]	Slope degree, Slope aspect, Altitude, Lithology, Distance to faults, Distance to rivers, Distance to roads, TWI, SPI, Slope Length, Land use, Plan Curvature	Topographic Maps of Scale 1:25,000 with 10 m contour interval	Index of Entropy and Conditional probability models in GIS	Index of Entropy (IoE) model performed slightly better than conditional probability. **Validation Results**: IOE model ~86.08%, CP model ~82.75%,
Oh et al., (2012) [107]	Slope, Aspect, Curvature, Lineaments, Land cover and NDVI	Aster imagery	Frequency Ratio and Logistic Regression Model	Landslide susceptibility map produced by ASTER DEM is reasonably good with observed accuracy of 25.77 m RMSE. Therefore, ASTER imagery could be exploited for susceptibility. **Validation Results**: FR model ~84.78%, LR model ~84.20%,
Jaboyedoff	Slope, Curvature,	LiDAR derived DEM	Review for landslide, rock fall and debris	High resolution DEMs are increasingly being used in

et al., (2012) [134]	TRI, STI		flow	landslide community and LiDAR sensors will become a standard tool for landslide analysis in the coming years. However, it will need development of more sophisticated tools for data processing.
Bagherzadeh and Mansouri, (2013) [135]	Geology formations, slope angles, slope aspect, elevation, land use, land cover, mode of failure, rainfall data, drainage network	Digitization survey data, Topographic maps, Satellite images	Factor maps production, Analytic hierarchy process (AHP)	Landslides events are strongly correlated with the slope angle of the basin. Active landslide zones have a high correlation (R^2 = 0.769) to slope classes over 30° and 53.85% of the basin is prone to landslides.
Martha et al., (2013) [136]	Slope angle, Slope aspect, Land use, Geology, Lithology, Soil depth, Relative relief	Cartosat-I imagery data with 10 m resolution	Semi-automated methods from post-event satellite images, Weights-of-evidence method	Semi-automatically prepared inventories can be used for landslide hazard and risk assessment in a data-poor environment.
Pawluszek and Borkowski, (2016) [103]	Elevation, Slope, Morphological gradient, Aspect, Area Solar Radiation, TRI, TWI, TPI, SPI, Shaded relief, Lithology, Distance to road, Drainage networks, Land use	LiDAR derived DEM	Principal component analyses, Weights assignment through Analytical Hierarchy Process (AHP)	Topographic factors play a significant role in landslide susceptibility, however AHP enhanced the results substantially, while adding lithology and environmental factors.
B Pradhan and Sameen, (2017) [109]	Slope, Aspect, Altitude, TWI, TRI, NDVI, Vegetation density, Land use, Distance to road, Distance to river, Distance to fault, Plan curvature, Profile Curvature	LiDAR based DEMs, ASTER based DEMs	ROC method, Kappa coefficient, Landslide density graphs, Multicollinearity analysis, Sensitivity analysis	No significant differences have been observed among the prediction and success rates for spatial resolution less than 10 m. LiDAR DEM contains more information even if it has been resampled from 0.5 m DEM. Optimal spatial resolution is 2 m based on the accuracy metrics. **Overall Accuracy**: ASTER DEM = 82.29% LiDAR DEM = 94.02%
Oh et al., (2018) [77]	Slope, Plan curvature, Aspect, TPI, TRI, SPI, TWI, thickness, slope length, Land use, Tree diameter, Tree age, Forest density, Convexity, Mid-Slope position	Topographic maps of scale 1:5000 with 5 m contour interval	Evidential Belief function (EBF), Logistic Regression (LR), Support Vector Machine (SVM) models	Training accuracy and prediction accuracy of the LR model was higher than the EBF and SVM model. **Validation Results**: EBF model ~92.25%, LR model ~94.59%, SVM model ~81.78%
A. Zhu et al., (2018) [137]	Elevation, Slope, Aspect, Plan Curvature, Profile Curvature, Distance to rivers, Distance to road, Lithology, Distance to faults, Land Cover	Topographic maps of scale 1:50,000	Presence-only method, Presence-absence method, Support Vector Machine (SVM), Kernel Density Estimation (KDE), Artificial Neural Networks (ANN)	Two-class SVM method has the best performance in susceptibility study among the applied methods. Landslide absence data method controlled the over-prediction of the models. **Validation Results**: 1class-SVM ~70.50%, KDE ~ 72.00%, ANN ~92.90% 2class-SVM ~95.10%
Dou et al., (2019) [138]	Slope angle, Slope aspect, Curvature, Distance to drainage network, Drainage density	Satellite imagery based DEM with spatial resolution of 10 m	Advanced Random Forest (RF) and Decision Tree (DT) algorithms	Methods were tested for rainfall-induced landslide susceptibility and overall efficiency of ARF is found better the DT results.

				Validation Results: ARF model ~95.60%, DT model ~92.80%
Juliev et al., (2019) [105]	Slope, Aspect, Elevation, Distance to Lineaments, Geology, Soil, Land use, Land cover, Distance to faults, Distance to roads, Distance to streams	ASTER30 DEM	Statistical Index (SI), Frequency Ratio (FR) and Certainty Factor (CF) model	Landslide susceptibility maps were categorized into five classes i.e., very low, low, moderate, high and very high. Training and prediction accuracies for SI remained higher than the other models. **Validation Results**: SI ~80%, FR ~70%, CF ~71%

5. Concluding Remarks and Future Perspectives

DEM development from different sources with required accuracy is an intricate process and needs lots of care. Landslide susceptibility based on DEMs, starts from the DEM development, parameters' derivation from them and attachment of additional landslide-conditioning factors, which are all not easy and simple tasks. However, DEMs have facilitated the researchers for risk assessment of landslide hazards by estimating the probability of landslide event using derived topographic attributes. Landslide hazards susceptibility mapping depends on the quality of utilized DEMs, targeted parameters, and adopted models, therefore it is a sensitive process and its implications towards human settlements and life makes it even more sensitive. Slope angle is declared as the most influential factor for landslide susceptibility among all other factors. Parameters associated with DEMs are mostly interconnected and dependent on their resolution e.g., slope angles are highly dependent upon DEM resolution. The ideal resolution of a DEM used for landslide risk assessment studies is considered to be resolution <10 m. Parameters involved in susceptibility mapping together with different DEMs data sources using different models or algorithms are discussed. A trend towards increasing the number of parameters or landslide conditioning factors along with the mixing of various models or methods will enhance the truthfulness of landslide susceptibility further. Parameters or conditioning factors derived from DEMs are responsible for zonal mapping of areas vulnerable for landslide hazard events in the future. Inventory lists include landslide-conditioning parameters derived from or used in addition to DEMs to identify the regions prone to such events. Geological and environmental parameters are additional and attached with each cell of DEMs to make landslide susceptibility mapping more precise. This study proposed two parameters to be used with DEMs for refinement of landslide susceptibility. Based on literature reviewed in this paper, future perspectives in this field are described here;

- Liquefaction is a phenomenon, usually triggered by the earthquakes and is considered as a disaster alone. Soil liquefaction is accompanied by the landslide events in hilly areas after an earthquake and depends on water quantity within the soil particles and soil type of that area [139]. Landslides occur in hilly areas, therefore it is a complicated task to attach ground water conditions to each cell in a DEM. Moreover, to achieve the true shape of hilly region, high resolution DEM is also necessary, which demands an abundance of field work to collect data for postulation of ground water conditions. Ground liquefaction is itself a disaster and related to groundwater conditions; therefore, we purpose that ground water condition can be an interesting conditioning factor or landslide inventory-parameter for susceptibility. It will be helpful if ground water or the landfill conditions are indexed with each cell of DEM for landslide risk assessments in the future.
- Deforestation or cutting the existing plantations (change in land cover) might be a factor for impact assessment of landslide events to quantify spatial extent of landslide event. Therefore, deforestation information of an area that is likely to be hit by a landslide event should be used with the DEMs to ascertain the spatial extent of landslide debris movement in future. Deforestation rates in this particular region can be quantified and used with a DEM to assess the spatial-extent of landslide event before it occurs.

Landslide events depend upon the topography of area and, to assess their risk in a digital environment, DEMs are basic and useful source of information related with the terrain topography. This information is further exploited in susceptibility studies and for risk assessment of such hazards. Areas identified in result of statistical analysis of the topographic parameters obtained from DEMs or attached with them using several models or methods, should be eluded for future development or if necessary than special measurements should be adopted to avoid effects (especially human life loss) of such disasters in future. Topographical, environmental, geological and lithological parameters have been used extensively previously by developing models and algorithms for susceptibility studies. However, due to rapid climate change of the Earth and other

related disasters, the probability of landslide hazards and other hazards has increased; therefore, it is emphasized that more and more such parameters or landslide conditioning factors should be studied in future for their evaluation and refinement of susceptibility mapping. This discussion will conclude with the argument that in the last two decades, major advancements can be seen in the field of landslide susceptibility, risk assessment and management. Parameters of ground water conditions and deforestation rate can be linked to DEMs (Figure 7) as landslide-conditioning factors and risk-assessment factors, respectively.

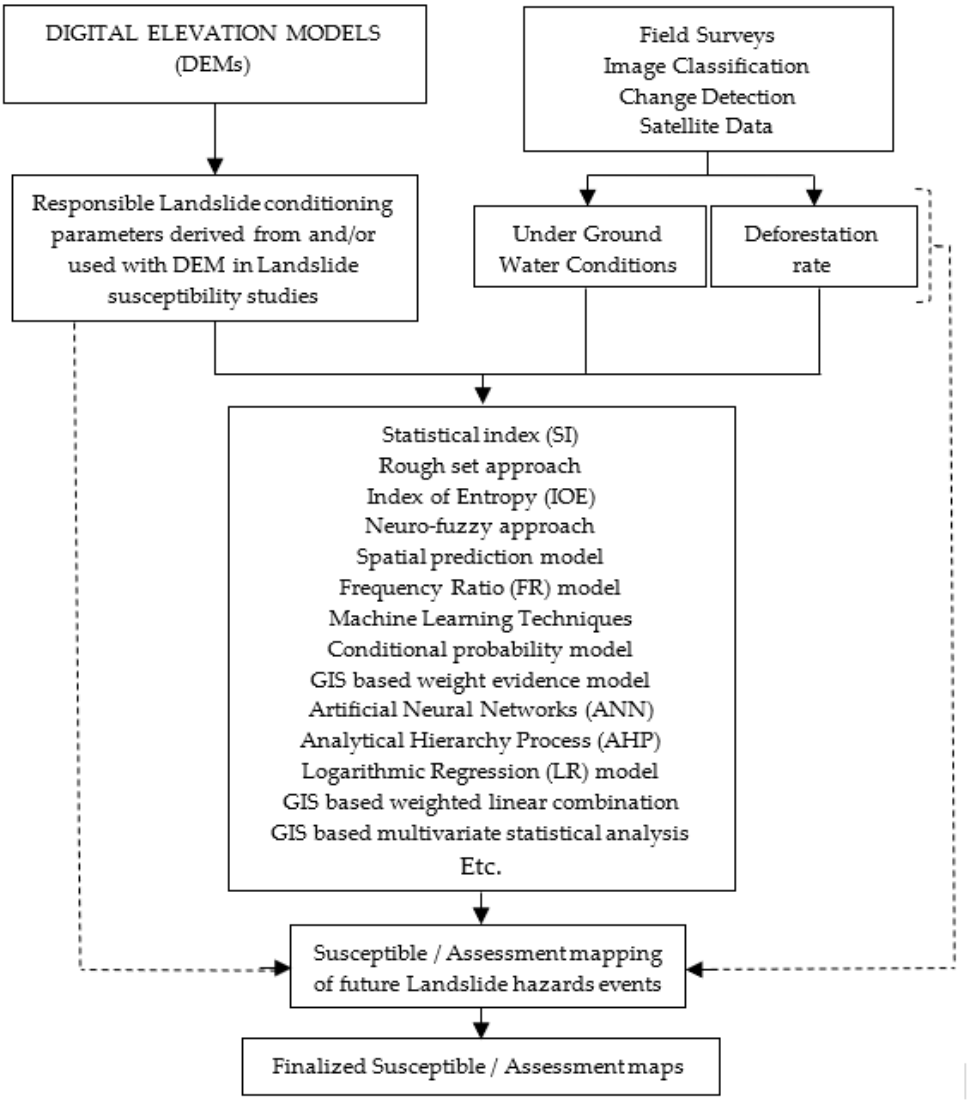

Figure 7. Conceptual framework for inclusion of proposed landslide conditioning factors/parameters for landslide susceptibility mapping and landslide risk assessment.

Author Contributions: Conceptualization, Nayyer Saleem; analysis, Nayyer Saleem and Md. Enamul Huq; investigation, Md. Enamul Huq and Nana Yaw Danquah Twumasi; resources, Nayyer Saleem; writing—original draft preparation, Nayyer Saleem; writing—review and editing, Nayyer Saleem and Asif Sajjad; visualization, Nana Yaw Danquah Twumasi and Asif Sajjad; supervision, Md. Enamul Huq; funding acquisition, Nayyer Saleem.

Funding: This work was supported in part by the National Key R and D plan on strategic international scientific and technological innovation cooperation special project under Grant 2016YFE0202300, the National

Natural Science Foundation of China under Grants 61671332, 41771452, and 41771454, the Natural Science Fund of Hubei Province in China under Grant 2018CFA007.

Acknowledgments: The authors would like to thank Prof. Stephen for helping us in English correction during revision.

Conflicts of Interest: The authors declare no conflict of interest.

References

1. Terrain Analysis. Dictionary of Military and Associated Terms. 2005. Available online: https://www.thefreedictionary.com/terrain+analysis (accessed on 25 August 2019).
2. Deng, Y.; Wilson, J.P.; Gallant, J.C. Chapter 23: Terrain Analysis. In *The Handbook of Geographic Information Science*; 1st ed.; John P. Wilson, A. Stewart Fotheringham, Eds; John Wiley & Sons, New York, USA:, 2008; pp. 417–435.
3. Mutluoglu, O. Investigation of the effect of land slope on the accuracy of digital elevation model (DEM) generated from various sources. *Sci. Res. Essays* **2010**, *5*, 1384–1391.
4. Toz, G.; Erdogan, M. DEM (Digital Elevation Model) Production and Accuracy Modeling of DEMs from 1: 35000 scale aerial photographs. In *The International Archives of the Photogrammetry, Remote Sensing and Spatial Information Sciences;* ISPRS, Beijing, China, 2008; Volume XXXVI, pp. 775–780.
5. Yakar, M. Digital Elevation Model Generation by Robotic Total Station Instrument. *Soc. Exp. Mech.* **2009**, *33*, 52–59.
6. Li, X.; Shen, H.; Feng, R.; Li, J.; Zhang, L. DEM generation from contours and a low-resolution DEM. *ISPRS J. Photogramm. Remote Sens.* **2017**, *134*, 135–147.
7. USGS. Available online: https://www.usgs.gov/ (accessed on14 August 2019).
8. Taud, H.; Parrot, J.; Alvarez, R. DEM generation by contour line dilation p. *Comput. Geosci.* **1999**, *25*, 775–783.
9. Li, Z.; Gold, Q.Z.C. *Digital Terrain Modeling: Principles and Methodology*; CRC Press, New York, USA: 2005.
10. Peralvo, M. Influence of DEM interpolation methods in drainage analysis. *GIS Water Resour.* **2004**, *4*, 26.
11. Vaze, J., and J. Teng. 2007. High-resolution LiDAR DEM: How good is it? In Proc. MODSIM 2007: Intl. Congress on Modelling and Simulation, 692-698. L. Oxley and D. Kulasiri, eds. Modelling and Simulation Society of Australia and New Zealand. Available at: www.mssanz.org.au/MODSIM07/ papers/12_s27/HighResolution_s27_Vaze_.pdf.
12. Arrighi, P.; Soille, P. From scanned topographic maps to digital elevation models. In *International Symposium on Imaging Applications in Geology*; D. Jongmans, E. Pirard, and P. Trefois Eds., Liege, Belgium, 1999; pp. 1–4.
13. Carter, J.R. Digital Representations of Topographic Surfaces. *Photogramm. Eng. Remote Sens.* **1988**, *54*, 1577–1580.
14. Soycan, A.; Soycan, M. Digital Elevation Model Production from Scanned Topographic conotur maps via Thin Plate Spline Interpolation. *Arab. J. Sci. Eng.* **2009**, *34*, 121–134.
15. Oky, P.; Yokoyama, D.A.R. DEM generation method from contour lines based on the steepest slope segment chain and a monotone interpolation function. *ISPRS J. Photogramm. Remote Sens.* **2002**, *57*, 86–101.
16. NASA JPL ASTER. Available online: https://asterweb.jpl.nasa.gov/gdem.asp (accessed on 5 October 2019).
17. Farr, T.G.; Rosen, P.A.; Caro, E.; Crippen, R.; Duren, R.; Hensley, S.; Kobrick, M.; Paller, M.; Rodriguez, E.; Roth, L.; et al. The Shuttle Radar Topography Mission. *Rev. Geophys.* **2007**, *45*, 1–33.
18. USGS. EROS Archive. Available online: https://www.usgs.gov/centers/eros/science/usgs-eros-archive-digital-elevation-global-30-arc-second-elevation-gtopo30?qt-science_center_objects=0#qt-science_center_objects (accessed on 5 October 2019).
19. Visser, P.N.A.M. Gravity field determination with GOCE and GRACE. *Adv. Sp. Res.* **1999**, *23*, 771–776.
20. NGA. Available online: https://www.nga.mil/ProductsServices/GeodesyandGeophysics/Pages/EarthGravityModel.aspx (accessed on 5 October 2019).
21. Balmino, G.; Vales, N.; Briais, S.B.A. Spherical harmonic modelling to ultra-high degree of Bouguer and isostatic anomalies. *J. Geod.* **2011**, *86*, 499–520.
22. Wang, T.; Belle, I.; Hassler, U. Modelling of Singapore s topographic transformation based on DEMs. *Geomorphology* **2015**, *231*, 367–375.

23. Fisher, P.F.; Tate, N.J. Causes and consequences of error in digital elevation models. *Prog. Phys. Geogr.* **2006**, *30*, 467–489.
24. Mercer, B. DEMs created from airborne IFSAR–An update. *Int. Arch. Photogramm. Remote Sens.* **2004**, *35*, pp. 242–248.
25. Hahn, M.; Samadzadegan, F. Integration of DTMs using wavelets. *Int. Arch. Photogramm. Remote Sens.* **1999**, *32*, 3–4.
26. Weng, Q. Quantifying Uncertainty of Digital Elevation Models Derived from Topographic Maps. In *Symposium on Advances in Spatial Data Handling*; 2002; D. Richardson, P. van Oosterom, Eds., Springer, Berlin, Heidelberg; pp. 403–418.
27. Chang, H.; Ge, L.; Rizos, C. Assessment of digital elevation models using RTK GPS. *J. Geospatial Eng.* **2004**, *6*, 1–8.
28. Webster, T.L.; Murphy, J.B.; Gosse, J.C.; Spooner, I. The application of lidar-derived digital elevation model analysis to geological mapping: An example from the Fundy Basin, Nova Scotia, Canada. *Can. J. Remote Sens.* **2006**, *32*, 173–193.
29. Zhang, C.; Fraser, C. Generation of Digital Surface Model From High Resolution. In *The International Archives of the Photogrammetry, Remote Sensing and Spatial Information Sciences;* ISPRS, Beijing, China, 2008; Volume XXXVI; pp. 785–790.
30. Capaldo, P.; Crespi, M.; Fratarcangeli, F.; Nascetti, A.; Francesca, P.; Agugiaro, G.; Poli, D.; Remondino, F. DSM Generation from Optical and SAR high resolution satellite Imagery: Methodology, Problems and Potentialities. In Proceedings of the International Geoscience Remote Sensing Symposium (IGARSS); Munich, Germany, 22–27 July, 2012; pp. 6936–6939.
31. Mohd, W.; Wan, N.M.A. Abdullah; Hashim, S. Evaluation of Vertical Accuracy of Digital Elevation Models Generated from Different Sources: Case Study of Ampang and Hulu Langat, Malaysia. *FIG Congress* **2014**, Volume XXV, pp. 1–17.
32. Wu, B.; Tang, S.; Zhu, Q.; Tong, K.; Hu, H.; Li, G. Geometric integration of high-resolution satellite imagery and airborne LiDAR data for improved geopositioning accuracy in metropolitan areas. *ISPRS J. Photogramm. Remote Sens.* **2015**, *109*, 139–151.
33. Yu, M.; Huang, Y.; Xu, Q.; Guo, P.; Dai, Z. Application of virtual earth in 3D terrain modeling to visual analysis of large-scale geological disasters in mountainous areas. *Environ. Earth Sci.* **2016**, *75*, 562–568.
34. Leitão, J.P.; de Sousa, L.M. Towards the optimal fusion of high-resolution Digital Elevation Models for detailed urban flood assessment. *J. Hydrol.* **2018**, *561*, 651–661.
35. Akturk, E.; Altunel, A.O. Accuracy Assesment of a Low-Cost UAV Derived Digital Elevation Model (DEM) in a Highly Broken and Vegetated Terrain. *Measurement* **2018**, *136*, 382–386.
36. UNITED NATIONS-SPIDER. Available online: https://www.un-spider.org (accessed on 20 August 2019).
37. UNITED NATIONS-OOSA. Available online: https://www.unoosa. org (accessed on 18 August 2019).
38. Altan, O.; Backhause, R.; Boccardo, P.; van Manen, N.; Trinder, J.; Zlatanova, S. *The Value of Geoinformation for Disaster Risk Management (VALID) Benefit Analysis Stakeholder Assessment*, 1st ed.; Joint Board of Geospatial Information Societies (JBGIS): Copenhagen, Denmark, 2013.
39. Altan, O. Use of Photogrammetry , Remote Sensing and Spatial Information Technologies in Disaster Management , especially Earthquakes. In *Geo-Information for Disaster Management*; van Oosterom, F.E.M., Zlatanova S, P., Eds.; Springer: Berlin/Heidelberg, Germany, 2005.
40. Li, D.; Shan, J.; Shao, Z.; Zhou, X.; Yao, Y. Geomatics for smart cities-concept, key techniques, and applications. *Geo-Spatial Inf. Sci.* **2013**, *16*, 13–24.
41. Li, D.; Shao, Z. The new era for geo-information. *Sci. China Ser. F Inf. Sci.* **2009**, *52*, 1233–1242.
42. Kocaman, S.; Gokceoglu, C. A CitSci app for landslide data collection. *Landslides* **2019**, *16*, 611–615.
43. Shao, Z.; Fu, H.; Li, D.; Altan, O.; Cheng, T. Remote sensing monitoring of multi-scale watersheds impermeability for urban hydrological evaluation. *Remote Sens. Environ.* **2019**, *232*, 111338.
44. Li, D.; Yao, Y.; Shao, Z.; Wang, L. From digital Earth to smart Earth. *Chin. Sci. Bull.* **2014**, *59*, 722–733.
45. Erasmi, S.; Rosenbauer, R.; Buchbach, R.; Busche, T.; Rutishauser, S. Evaluating the quality and accuracy of TanDEM-X digital elevation models at archaeological sites in the Cilician Plain, Turkey. *Remote Sens.* **2014**, *6*, 9475–9493.
46. Alganci, U.; Besol, B.; Sertel, E. Accuracy Assessment of Different Digital Surface Models. *ISPRS Int. J. Geo-Information* **2018**, *7*, 16.

47. Li, D.; Ma, J.; Cheng, T.; Genderen, J.L.V.; Shao, Z. Challenges and opportunities for the development of MEGACITIES. *Int. J. Digit. Earth* **2018**, *12*, 1382–1395.
48. IFRC. Available online: https://www.ifrc.org/en/what-we-do/disaster-management/about-disasters/what-is-a-disaster/ (accessed on 24 August 2019).
49. Cruden, M.D. A Simple Definition of a Landslide. *Int. Assoc. Eng. Geol.* **1991**, *43*, 27–29.
50. Nadim, F.; Kjekstad, O.; Peduzzi, P.; Herold, C.; Jaedicke, C. Global landslide and avalanche hotspots. *Landslides* **2006**, *3*, 159–173.
51. Gorum, T.; Fan, X.; van Westen, C.J.; Huang, R.Q.; Xu, Q.; Tang, C.; Wang, G. Geomorphology Distribution pattern of earthquake-induced landslides triggered by the 12 May 2008 Wenchuan earthquake. *Geomorphology* **2011**, *133*, 152–167.
52. Crosta, G.; Imposimato, S.; Roddeman, D.; Chiesa, S.; Moia, F. Small fast-moving flow-like landslides in volcanic deposits: The 2001 Las Colinas Landslide (El Salvador). *Eng. Geol.* **2005**, *79*, 185–214.
53. Chigira, M.; Wu, X.; Inokuchi, T.; Wang, G. Landslides induced by the 2008 Wenchuan earthquake, Sichuan, China. *Geomorphology* **2010**, *118*, 225–238.
54. Scientific Visualization Studio (NASA). Available online: https://svs.gsfc.nasa.gov/4710 (accessed on 31 August 2019).
55. Moore, I.D.; Grayson, R.B.; Ladson, A.R. Digital Terrain Modeling: A review of Hydrological, Geomorphological and Biological applications. *Hydrol. Process.* **1991**, *5*, 3–30.
56. Wolock, D.; Price, C.V. Effect of Digital Elevation Model Map Scale and Data Resolution on a Topography-Based Watershed Model. *Water Resour. Res.* **1994**, *30*, 3041–3052.
57. Lee, E.M.; Jones, D.K.C. *Landslide Risk Assessment*, 1st ed.; Thomas Telford Publishing: London, UK; 1 Heron Quay: London, UK, 2004.
58. Gao, J. Identification of topographic settings conducive to landsliding from DEM in Nelson county, Virginia, U.S.A. *Earth Surf. Process. Landf.* **1993**, *18*, 579–591.
59. Cardinali, M.; Reichenbach, P.; Guzzetti, F.; Ardizzone, F.; Antonini, G.; Galli, M.; Cacciano, M.; Castellani, M.; Salvati, P. System Sciences A geomorphological approach to the estimation of landslide hazards and risks in Umbria , Central Italy. *Nat. Hazards Earth Syst. Sci.* **2002**, *2*, 57–72.
60. Costanzo, D.; Rotigliano, E.; Irigaray, C.; Jim, J.D. Factors selection in landslide susceptibility modelling on large scale following the gis matrix method: Application to the river Beiro basin (Spain). *Nat. Hazards Earth Syst. Sci.* **2012**, *12*, 327–340.
61. Fenton, G.A.; McLean, A.; Nadim, F.; Griffiths, D.V. Landslide hazard assessment using digital elevation models. *Can. Geotech. J.* **2013**, *50*, 620–631.
62. Lines, F. Chapter 5: Curvature. In *Geometry for Naval Architects*; 1st ed.; A. Biran, Eds; Elsevier Ltd, The Netherlands, 2019; pp. 223–257.
63. Stump, S. Secondary Mathematics Teachers' Knowledge of Slope. *Math. Educ. Res. J.* **1999**, *11*, 124–144.
64. Horn, B.K.P. Understanding Image Intensities. *Artif. Intell.* **1977**, *8*, 201–231.
65. Horn, B.K.P. Hill Shading and the Reflectance Map. *Proc. IEEE* **1981**, *69*, 14–47.
66. Burrough, P.A. *Principles of Geographical Information Systems for Land Resources Asessment*, 1st ed.; Clarendon Press: Oxford, UK, 1986.
67. Skidmore, A.K. A comparison of techniques for calculating gradient and aspect from a gridded digital elevation model. *Int. J. Geogr. Inf. Syst.* **1989**, *3*, 323–334.
68. Raaflaub, L.D.; Collins, M.J. The effect of error in gridded digital elevation models on the estimation of topographic parameters. *Environ. Model. Softw.* **2006**, *21*, 710–732.
69. Mclean, A. *Landslide Risk Assessment Using Digital Elevation Models*; Dalhousie University: Halifax, Nova Scotia, 2011.
70. Zevenbergen, L.W.; Thorne, C.R. Quantitative Analysis of Land Surface Topography. *Earth Surf. Dyn.* **1987**, *12*, 47–56.
71. Lee, S.; Ryu, J.H.; Won, J.S.; Park, H.J. Determination and application of the weights for landslide susceptibility mapping using an artificial neural network. *Eng. Geol.* **2004**, *71*, 289–302.
72. Rasyid, A.R.; Bhandary, N.P.; Yatabe, R. Performance of frequency ratio and logistic regression model in creating GIS based landslides susceptibility map at Lompobattang Mountain , Indonesia. *Geoenvironmental Disasters* **2016**, *3*, 1–16.

73. ArcMap: Curvature Function. Available online: http://desktop.arcgis.com/en/arcmap/10.3/manage-data/raster-and-images/curvature-function.htm (accessed on 28 August 2019).
74. Guisan, A.; Weiss, S.B.; Weiss, A.D. GLM versus CCA spatial modeling of plant species distribution. *Plant Ecol.* **1999**, *143*, 107–122.
75. Weiss, A.D. Topographic Position and Landforms Analysis. In Proceedings of the Poster Presentation at ESRI User Conference, Seattle, Washington, USA, 22–24 January, 2001.
76. Jebur, M.N.; Pradhan, B.; Tehrany, M.S. Remote Sensing of Environment Optimization of landslide conditioning factors using very high-resolution airborne laser scanning (LiDAR) data at catchment scale. *Remote Sens. Environ.* **2014**, *152*, 150–165.
77. Oh, H.; Kadavi, P.R.; Lee, C.; Lee, S. Evaluation of landslide susceptibility mapping by evidential belief function , logistic regression and support vector machine models. *Geomatics, Nat. Hazards Risk* **2018**, *9*, 1053–1070.
78. Jenness, J.; Brost, B.; Beier, P. *Land Facet Corridor Designer*; USDA Forest Service Rocky Mountain Research Station,; Arizona, USA 2013.
79. Enterprises, J. 2019. Available online: http://www.jennessent.com/arcgis/arcgis_extensions.htm (accessed on 8 Sepmber 2019).
80. Jiang, L.; Ling, D.; Zhao, M.; Wang, C.; Liang, Q.; Liu, K. Effective Identification of Terrain Positions from Gridded DEM Data Using Multimodal Classification Integration. *ISPRS Int. J. Geo-Inf.* **2018**, *7*, 443.
81. Grabs, T.; Seibert, J.; Bishop, K.; Laudon, H. Modeling spatial patterns of saturated areas: A comparison of the topographic wetness index and a dynamic distributed model. *J. Hydrol.* **2009**, *373*, 15–23.
82. Grimm, K.; Nasab, M.T.; Chu, X. TWI Computations and Topographic Analysis of Depression-Dominated Surfaces. *Water* **2018**, *10*, 663.
83. Beven, K.J.; Kirkby, M.J. A physically based, variable contributing area model of basin hydrology/Un modèle à base physique de zone d'appel variable de l'hydrologie du bassin versant. *Hydrol. Sci. Bull.* **1979**, *24*, 43–69.
84. Schmidt, F. Comparison of DEM Data Capture and Topographic Wetness Indices. *Precis. Agric.* **2003**, *4*, 179–192.
85. Gu, A.; Seibert, J. Modeling Spatial Patterns of Saturated Areas: An Evaluation of Different Terrain Indices. *Water Resour. Res.* **2004**, 40,114–133.
86. Sørensen, R.; Zinko, U.; Seibert, J.; Sørensen, R.; Zinko, U.; On, J.S. On the calculation of the topographic wetness index: Evaluation of different methods based on field observations. *Hydrol. Earth Syst. Sci. Discuss. Eur. Geosci. Union* **2006**, *10*, 101–112.
87. Zhu, C.Q.A.; Pei, T.; Thomas, B.L. An approach to computing topographic wetness index based on maximum downslope gradient. *Precis. Agric.* **2011**, *12*, 32–43.
88. Buchanan, B.P.; Fleming, M.; Schneider, R.L.; Richards, B.K.; Archibald, J.; Qiu, Z.; Walter, M.T. Evaluating topographic wetness indices across central New York agricultural landscapes. *Hydrol. Earth Syst. Sci.* **2014**, *18*, 3279–3299.
89. Smith, M.W. Roughness in the Earth Sciences. *Earth Sci. Rev.* **2014**, *136*, 202–225.
90. Korzeniowska, K.; Korup, O. *Mapping Gullies Using Terrain-Surface Roughness*; In the 19th AGILE conference on Geographic Information Science, Helsinki, Finland, 14-17 June, 2016; Springer.
91. Riley, J.S.; de Gloria, D.S.; Elliot, R. Terrain Ruggedness Index that Quantifies Topographic Heterogeneity. *Intermt. J. Sci.* **1999**, *5*, 23–27.
92. Shepard, M.K.; Campbell, B.A.; Bulmer, M.H.; Farr, T.G.; Gaddis, L.R.; Plaut, J.J. A planetary and remote sensing perspective. *J. Geophys. Res.* **2001**, *106*, 777–795.
93. Frankel, K.L.; Dolan, J.F. Characterizing arid region alluvial fan surface roughness with airborne laser swath mapping digital topographic data. *J. Geophys. Res.* **2007**, *112*, 1–14.
94. Cavalli, M.; Marchi, L. Characterisation of the surface morphology of an alpine alluvial fan using airborne LiDAR. *Nat. Hazards Earth Syst. Sci.* **2008**, *8*, 323–333.
95. Wenjie, L.; Danxun, L.; Xingkui, W. An approach to estimating sediment transport capacity of overland flow. *Sci. China Technol. Sci.* **2011**, *54*, 2649–2656.
96. Moore, I.D.; Burch, G.J. Sediment Transport Capacity of Sheet and Rill Flow: Application of Unit Stream Power Theory. *Water Resour. Res.* **1986**, *22*, 1350–1360.

97. Moore, I.D.; Wilson, J.P. Length-slope factors for the Revised Universal Soil Loss Equation: Simplified method of estimation. *J. Soil Water Conserv.* **1992**, *47*, 423–428.
98. Tayfur, G. Applicability of sediment transport capacity models for nonsteady state erosion from steep slopes. *J. Hydrol. Eng.* **2002**, *7*, 252–259.
99. Chandra, K.; Amar, D.; Regmi, D.; Reza, H.; Althuwaynee, O.F. Landslide susceptibility mapping using certainty factor , index of entropy and logistic regression models in GIS and their comparison at Mugling – Narayanghat road section in Nepal Himalaya. *Nat. Hazards* **2013**, *65*, 135–165.
100. Wang, Q.; Li, W.; Wu, Y.; Pei, Y.; Xie, P. Application of statistical index and index of entropy methods to landslide susceptibility assessment in Gongliu (Xinjiang, China). *Environ. Earth Sci.* **2016**, *75*, 598–610.
101. Moore, I.D. A Contour-based Topographic Model for Hydrological and Ecological Applications. *Earth Surf. Process. Landf.* **1988**, *13*, 305–320.
102. Pradhan, B.; Sezer, E.A.; Gokceoglu, C.; Buchroithner, M.F. Landslide susceptibility mapping by neuro-fuzzy approach in a landslide-prone area (Cameron Highlands, Malaysia). *IEEE Trans. Geosci. Remote Sens.* **2010**, *48*, 4164–4177.
103. Pawluszek, K.; Borkowski, A. Impact of DEM-derived factors and analytical hierarchy process on landslide susceptibility mapping in the region of Roznow Lake, Poland. *Nat. Hazards* **2016**, *86*, 919–952.
104. Yilmaz, I. Landslide susceptibility mapping using frequency ratio, logistic regression, artificial neural networks and their comparison: A case study from Kat landslides (Tokat—Turkey). *Comput. Geosci.* **2009**, *35*, 1125–1138.
105. Juliev, M.; Mergili, M.; Mondal, I.; Nurtaev, B.; Pulatov, A.; Hübl, J. Comparative analysis of statistical methods for landslide susceptibility mapping in the Bostanlik District, Uzbekistan. *Sci. Total Environ.* **2019**, *653*, 801–814.
106. Lee, S.; Talib, J.A. Probabilistic landslide susceptibility and factor effect analysis. *Environ. Geol.* **2005**, *47*, 982–990.
107. Oh, H.; Park, N.; Lee, S.; Lee, S. Extraction of landslide-related factors from ASTER imagery and its application to landslide susceptibility mapping. *Int. J. Remote Sens.* **2012**, *33*, 3211–3231.
108. Dlugosz, M. Digital Terrain Model (DTM) As a Tool for Landslide Investigation in the Polish Carpathians. *Versita* **2012**, *XLVI*, 5–23.
109. Pradhan, B.; Sameen, M.I. Effects of the Spatial Resolution of Digital Elevation Models and their Products on Landslide Susceptibility Mapping. *Laser Scanning Applications in Landslide Assessment*; **2017**; 2, 133–150.
110. Deng, Y.; Wilson, J.P.; Bauer, B.O. DEM resolution dependencies of terrain attributes across a landscape. *Int. J. Geogr. Inf. Sci.* **2007**, *21*, 187–213.
111. Vaze, J.; Teng, J.; Spencer, G. Impact of DEM accuracy and resolution on topographic indices. *Environ. Model. Softw.* **2010**, *25*, 1086–1098.
112. Chow, T.E.; Hodgson, M.E. Effects of lidar post-spacing and DEM resolution to mean slope estimation. *Int. J. Geogr. Inf. Sci.* **2009**, *23*, 1277–1295.
113. Ciampalini, A.; Raspini, F.; Frodella, W.; Bardi, F.; Bianchini, S.; Moretti, S. The effectiveness of high-resolution LiDAR data combined with PSInSAR data in landslide study. *Landslides* **2016**, *13*, 399–410.
114. Pesci, A.; Baldi, P.; Bedin, A.; Casula, G.; Cenni, N.; Fabris, M.; Loddo, F.; Mora, P.; Bacchetti, M. Digital elevation models for landslide evolution monitoring: Application on two areas located in the Reno River Valley (Italy). *Ann. Geophys.* **2004**, *47*, 1339–1353.
115. Mahalingam, R.; Olsen, M.J.; Banion, M.S.O. Evaluation of landslide susceptibility mapping techniques using lidar-derived conditioning factors (Oregon case study). *Geomat. Nat. Hazards Risk* **2016**, *7*, 1884–1907.
116. Chang, K.T.; Dou, J.; Chang, Y.; Kuo, C.P.; Xu, K.M.; Liu, J.K. Spatial resolution effects of digital terrain models on landslide susceptibility analysis. In *The International Archives of the Photogrammetry, Remote Sensing Spatial Information Sciences*; L. Halounova, V. Šafář, P. L. N. Raju, L. Plánka, V. Ždímal, T. Srinivasa Kumar, F. S. Faruque, Y. Kerr, S. M. Ramasamy, J. Comiso, Y. A. (Yousif) Hussin, P. S. Thenkabail, S. Lavender, A. Skidmore, P. Yue, P. Patias, O. Altan, and Q. Weng, Eds,; ISPRS Archives; Prague, Czech Republic, 12–19 July, 2016; Volume XLI-B8, pp. 33–36.
117. Wang, B.; Shi, W.; Liu, E. Robust methods for assessing the accuracy of linear interpolated DEM. *Int. J. Appl. Earth Obs. Geoinf.* **2015**, *34*, 198–206.
118. Carrara, A.; Guzzetti, F.; Cardinali, M.; Reichenbach, P. Use of GIS Technology in the Prediction and Monitoring of Landslide Hazard. *Nat. Hazards* **1999**, *20*, 117–135.

119. Ercanoglu, M.; Gokceoglu, C. Use of fuzzy relations to produce landslide susceptibility map of a landslide prone area (West Black Sea Region, Turkey). *Eng. Geol.* **2004**, *75*, 229–250.
120. Gorsevski, P.V.; Jankowski, P. Discerning landslide susceptibility using rough sets. *Comput. Environ. Urban Syst.* **2008**, *32*, 53–65.
121. Yesilnacar, E.; Topal, T. Landslide susceptibility mapping: A comparison of logistic regression and neural networks methods in a medium scale study , Hendek region (Turkey). *Eng. Geol.* **2005**, *79*, 251–266.
122. Kawabata, D.; Bandibas, J. Geomorphology Landslide susceptibility mapping using geological data , a DEM from ASTER images and an Arti fi cial Neural Network (ANN). *Geomorphology* **2009**, *113*, 97–109.
123. Xiaolong, D.; Li, L.; Tan, Y. Validation of spatial prediction models for landslide susceptibility mapping by considering structural similarity. *ISPRS Int. J. Geo-Inf.* **2017**, *6*,103.
124. Liu, X.; Miao, C. Large-scale assessment of landslide hazard , vulnerability and risk in China. *Geomatics, Nat. Hazards Risk* **2018**, *9*, 1037–1052.
125. Dagdelenler, G.; Nefeslioglu, H.A.; Gokceoglu, C. Modification of seed cell sampling strategy for landslide susceptibility mapping: An application from the Eastern part of the Gallipoli Peninsula (Canakkale, Turkey). *Bull. Eng. Geol. Environ.* **2015**, *75*, 575–590.
126. Liu, J.; Duan, Z. Quantitative assessment of landslide susceptibility comparing statistical index, index of entropy, and weights of evidence in the Shangnan Area, China. *Entropy* **2018**, *20*, 9–11.
127. Sadisun, I.A.; Arifianti, Y. Weights of Evidence Method for Landslide Susceptibility Mapping in Takengon, Central Aceh, Indonesia. In Proceedings of the IOP Conference Series: Earth Environmental Science, Bandung, Indonesia, 18–19 October, 2017
128. Reichenbach, P.; Rossi, M.; Malamud, B.D.; Mihir, M.; Guzzetti, F. Earth-Science Reviews statistically-based landslide susceptibility models. *Earth-Sci. Rev.* **2018**, *180*, 60–91.
129. Chen, W.; Panahi, M.; Tsangaratos, P.; Shahabi, H.; Ilia, I.; Panahi, S.; Li, S.; Jaafari, A.; Ahmad, B.B. Applying population-based evolutionary algorithms and a neuro-fuzzy system for modeling landslide susceptibility. *Catena* **2019**, *172*, 212–231.
130. Carrara, A.; Cardinali, M.; Detti, R.; Guzzetti, F.; Pasqui, V.; Reichenbach, P. GIS techniques and statistical models in evaluating landslide hazard. *Earth Surf. Process. Landf.* **1991**, *16*, 427–445.
131. Nichol, J.; Wong, M.S. Satellite remote sensing for detailed landslide inventories using change detection and image fusion. *Int. J. Remote Sens.* **2005**, *26*, 1913–1926.
132. Miner, A.S.; Flentje, P.; Mazengarb, C.; Windle, D.J. Landslide Recognition using LiDAR derived Digital Elevation Models-Lessons learnt from selected Australian examples. In Proceedings of the Geologically Active Proceedings 11th IAEG Congregalia Auckland, New Zealand, 5–10 Septmber 2010; Volume 2010, p. 352.
133. Pourghasemi, H.R.; Mohammady, M.; Pradhan, B. Landslide susceptibility mapping using index of entropy and conditional probability models in GIS: Safarood Basin, Iran. *Catena* **2012**, *97*, 71–84.
134. Jaboyedoff, M.; Oppikofer, T.; Abellán, A.; Derron, Ma.; Loye, A.; Metzger, R.; Pedrazzini, A. Use of LIDAR in landslide investigations: A review. *Nat. Hazards* **2012**, *61*, 5–28.
135. Bagherzadeh, A.; Mansouri, M. Mapping of landslide hazard zonation using GIS at Golestan watershed , northeast of Iran. *Arab J. Geosci.* **2013**, *6*, 3377–3388.
136. Martha, T.R.; van Westen, C.J.; Kerle, N.; Jetten, V.; Kumar, K.V. Landslide hazard and risk assessment using semi-automatically created landslide inventories. *Geomorphology* **2013**, *184*, 139–150.
137. Zhu, A.; Miao, Y.; Yang, L.; Bai, S.; Liu, J. Comparison of the presence-only method and presence-absence method in landslide susceptibility mapping. *Catena* **2018**, *171*, 222–233.
138. Dou, J.; Yunus, A.P.; Bui, D.; Merghadi, A.; Sahana, M.; Zhu, Z.; Chen, Ch.; Khosravi, K.; Yang, Y.; ThaiPham, B. Assessment of advanced random forest and decision tree algorithms for modeling rainfall-induced landslide susceptibility in the Izu-Oshima Volcanic Island, Japan. *Sci. Total Environ.* **2019**, *662*, 332–346.
139. Massey, C.; van Dissen, R.; McSaveney, M.; Townsend, D.; Hancox, G.; Little, T.A.; Ries, W.; Perrin, N.; Archibald, G.; Dellow, G. *Landslides and Liquefaction Generated by the Cook Strait and Lake Grassmere Earthquakes*; A Reconnaissance Report: WEllington, New Zealand, 2013.